

BIOLOGICAL DEPOSITION OF IRON CATALYST
FOR CARBON NANOTUBE GROWTH

by

Mark Willis Esty

A senior thesis submitted to the faculty of

Brigham Young University

in partial fulfillment of the requirements for the degree of

Bachelor of Science

Department of Physics and Astronomy

Brigham Young University

April 2007

Copyright © 2007 Mark Willis Esty

All Rights Reserved

BRIGHAM YOUNG UNIVERSITY

DEPARTMENT APPROVAL

of a senior thesis submitted by

Mark Willis Esty

This thesis has been reviewed by the research advisor, research coordinator,
and department chair and has been found to be satisfactory.

Date

Richard Vanfleet, Advisor

Date

Eric Hintz, Research Coordinator

Date

Scott D. Sommerfeldt, Chair

ABSTRACT

BIOLOGICAL DEPOSITION OF IRON CATALYST FOR CARBON NANOTUBE GROWTH

Mark Willis Esty

Department of Physics and Astronomy

Bachelor of Science

The usefulness of ferritin as a catalyst in the chemical vapor deposition process for carbon nanotube growth is analyzed. It is found that restricting the ferritin deposition time and rinsing the sample reduced the density to a single, well-spaced layer which significantly decreases the amalgamation of the iron cores. The density of the deposited ferritin is found to be significantly affected by the choice of substrate. Annealing studies were done to simulate the nanotube growth conditions between 600°C and 800°C. The mobility of the iron cores during the annealing process is decreased by removing the protein shells of the ferritin molecules through exposure to an oxygen plasma prior to the anneal. The suggested process can minimize the spread in the catalyst diameters near 600°C; however, it is unlikely that this process can prevent the catalyst particles from amalgamating at temperatures near 800°C, where most nanotube growths are performed.

ACKNOWLEDGMENTS

I would like to thank Dr. Vanfleet for his extensive knowledge and his even more extensive patience. I would also like to thank Jeff Farrer, Daniel Richardson, David Cullen, Clark Blockburger, Jason Neff, and the other members of the TEM Research Group for their assistance in helping me to accomplish my research and keep sane in the lab. I would also like to acknowledge funding from the Department of Physics and Astronomy at BYU, the National Science Foundation's REU program at BYU, and BYU's Office of Research and Creative Activities.

Contents

Table of Contents	6
List of Figures	7
1 INTRODUCTION	1
1.1 Motivation for Research	1
1.2 Background of Carbon Nanotubes	2
1.3 Research in Diameter-Controlled Chemical-Vapor-Deposition Catalysts	3
1.4 Ferritin	5
1.5 Previous Research in Ferritin Catalysts	6
1.6 Research Goals	9
2 MATERIALS AND METHODS	10
2.1 Imaging Equipment	10
2.2 Early Experiments	12
2.3 Obstacles: Density, Movement, and Heat	15
2.4 Ferritin Deposition Process	15
2.5 Importance of Substrate on Density	16
2.6 Plasma Cleaning	18
2.7 Annealing Process	19
3 RESULTS AND CONCLUSIONS	20
3.1 Effect of Ferritin Proximity on Amalgamation	20
3.2 Effect of Plasma Cleaning	22
3.3 Diffusion Length	28
3.4 Conclusions	30
Bibliography	31
Index	33

List of Figures

1.1	Illustration of Carbon Nanotubes	2
1.2	The protein shell of a ferritin molecule	6
2.1	Tecnai F-20 Analytical STEM microscope	13
2.2	High density ferritin deposition	14
2.3	Large iron crystal	14
2.4	Ferritin concentration on silicon nitride	16
2.5	Ferritin concentration on carbon	17
2.6	Ferritin concentration on silicon dioxide	18
2.7	Image of the plasma cleaner	19
3.1	Small clusters and chains of ferritin molecules	21
3.2	A dense clump of ferritin	21
3.3	Large Iron crystals formed at 600°C	22
3.4	Ferritin clusters and chains before annealing	23
3.5	Ferritin clusters and chains after annealing	24
3.6	Discrete ferritin pair after annealing	25
3.7	Ferritin deposited on a silicon nitride surface	26
3.8	Disribution of iron cores after plasma cleaning	26
3.9	Plasma cleaned sample annealed at 600°C	27
3.10	Ferritin nanoparticles annealed at 600°C	28
3.11	Plasma cleaned sample annealed at 800°C	29

Chapter 1

INTRODUCTION

1.1 Motivation for Research

Carbon nanotubes have the potential to be among the most useful molecules in the history of science. Despite diameters that are only slightly larger than one nanometer, these tiny cylinders of carbon atoms have attracted interest from a variety of scientific disciplines as a result of their unique intrinsic characteristics. For example, carbon nanotubes' immense strength-to-weight ratio suggests their ability to create extremely strong and lightweight composites [1]; their hollow interiors suggests using them as nanoscopic syringes to deliver medicine directly to target cells [2]; and their ability to be either a metal or a semiconductor suggests using them as channels and gates in future transistor technologies [3]. Indeed, it seems like every day a new use is suggested for these "renaissance" molecules. However, most of these potential applications are hampered by researchers' inability to develop a growth process that can 1) produce carbon nanotubes with consistent characteristics and 2) control their placement within a larger system.

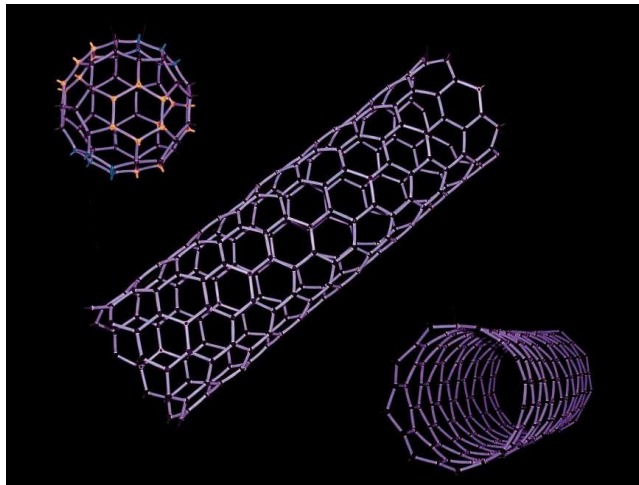


Figure 1.1 The sphere in the upper left is a depiction of a Buckminsterfullerene molecule (C₆₀). The other two images are an artist's depictions of single walled carbon nanotubes. (Graphic obtained from <http://spice.chem.emory.edu/students/welsher/nanotube.html>)

1.2 Background of Carbon Nanotubes

An introductory description of carbon nanotubes can be approached from either of two directions. First, carbon nanotubes can be viewed as individual Buckminsterfullerene molecules (elemental spheres of carbon discovered in 1985 [4]) that have been opened and elongated by addition of carbon atoms to form a cylindrical tube (Fig. 1.1). A second, and generally more useful, approach is to view them as single sheets of graphene (single atomic layers of graphite) that have been folded on themselves to form cylinders [5]. Some nanotubes contain many concentric cylinders of increasing diameters; these are known as multi-walled nanotubes. Single-Walled NanoTubes (SWNT) are generally between 1 nm and 3 nm in diameter. Multiwalled nanotubes are much thicker and generally have more structural defects. These defects alter the electrical and material properties of the multiwalled nanotubes and affect their usefulness in many applications. In this thesis, we focus almost exclusively on single-walled nanotubes.

Single-walled carbon nanotubes were first produced in 1993 by Sumio Iijima of the NEC Fundamental Research Laboratory in Japan [3]. Iijima produced these nanotubes by causing an electric arc discharge to occur between two graphite electrodes in a helium atmosphere [6]. Another process that is used to produce nanotubes was pioneered by Richard Smalley at Rice University. In this process nanotubes are created by “blasting a carbon target with an intense, pulsed laser beam” [6]. Both of these processes can produce relatively large quantities of bulk SWNT that can then be deposited on a surface or used in a solution.

The third major nanotube growth process, Chemical Vapor Deposition (CVD), allows more control over the placement of the nanotubes as they are grown. In CVD, a catalyst, usually a metal nanoparticle, is placed on a substrate and then heated to a temperature between 600-1000 °C while a carbon-rich gas, such as ethylene or methane, is blown over the surface. The high temperatures and actions of the catalyst cause the gas to decompose and dissolve in the metal catalyst. When the catalyst particles become saturated with carbon the carbon atoms precipitate and form carbon nanotubes [5,6]. Because it is more controllable than the other two processes, CVD has become the leading method for nanotube growth in research where precision placement of the nanotubes is important.

1.3 Research in Diameter-Controlled Chemical-Vapor-Deposition Catalysts

Although CVD shows promise, there are many obstacles to overcome before it can produce consistent SWNT growth. In CVD, the number, length, and chemical purity of the nanotubes can be affected by changes in the growth temperature, catalyst composition, growth pressure, substrate, and gas composition. All of these variables

are relatively easy to adjust.

However, the nanotubes' diameters are much more difficult to control. Control over this characteristic is very important since the diameters of the nanotubes have a close correlation with their helicity [7]. Helicity, or chirality, refers to the orientation of the graphene structure of a nanotube and determines whether the nanotube is metallic or semiconducting (see [5] for further details). In addition, the energy gaps of semiconducting nanotubes are inversely proportional to their diameters [5]. The nanotube diameters are very dependant on the size of the metal nanoparticle from which they were grown [8]. Many CVD growth experiments have contained fairly broad diameter distributions in the nanoparticles used as catalysts, which carried over into broad distributions in the diameters of the resultant nanotubes [7,8].

Lei An *et al.* used an organic capping agent to produce nearly identical nanoparticles containing 84 molybdenum atoms and 30 iron atoms [7]. They initially obtained relatively broad distributions in their nanotube diameters. They speculated that the nanoparticles were aggregating together to form larger catalyst particles. To reduce these problems they chemically modified the silicon-dioxide surface to anchor the nanoparticles to the substrate. With this technique they were able to obtain SWNT with diameters ranging from 0.7 to 1.5 nm, an average size of 1.0 nm and a standard deviation of 0.18 nm or 17 percent [7].

Another group, Ishida *et al.* in Tsukuba, Japan, used a combination of electron beam lithography and annealing to create nanoparticles of iron whose positions could be controlled with great accuracy (within 5 nm of a desired location) [9]. The nanotubes that were obtained by this method had an average diameter of 1.3 nm and a standard deviation of 0.4 nm. However, in this method nanotubes only grew from about 10 percent of the catalyst particles. This low particle-to-nanotube ratio highlights one of the quandaries of catalyst design. The nanotube yield can be in-

creased by altering the composition of the catalyst. However, to preserve consistency in the particle size, a new deposition process would need to be developed for each new composition.

In summary, an ideal CVD catalyst would: 1) have nanoparticle diameters that are both consistent and controllable, 2) have a metal composition that can be deliberately varied, 3) be easily available and relatively simple to process, and 4) allow control over its placement within a larger system.

1.4 Ferritin

The biological molecule ferritin has been suggested as a vehicle to produce a nanotube catalyst that approaches the ideal characteristics suggested above. The ferritin molecule is essential to the capture and storage of free iron in living organisms. Each ferritin is composed of a 10 to 12 nm protein shell that is approximately 2.5 nm thick (Fig. 1.2). This shell consists of 24 protein subunits which intersect to form channels where ferrous (Fe^{2+}) is oxidized to ferric (Fe^{3+}) which is then transported into the hollow center of the molecule where it is stored as $\text{Fe}(\text{OH})_3$. This stored iron can then be reduced and released as it is needed by the parent organism [10]. When the protein shell contains a metal core it is known as holo-ferritin. When the shell is empty it is known as apo-ferritin. For a detailed study of the ferritin molecule, we refer the reader to [10].

After ferritin has been obtained from a living organism, the iron cores can be removed by chemical means to produce apo-ferritin. A controlled quantity of metal atoms can then be added to the ferritin cores to produce reconstituted holo-ferritin [8, 11]. Due to: 1) the consistency of the biological shells and the narrow size distribution of the resultant cores, 2) the variety of metals that can be artificially implanted inside

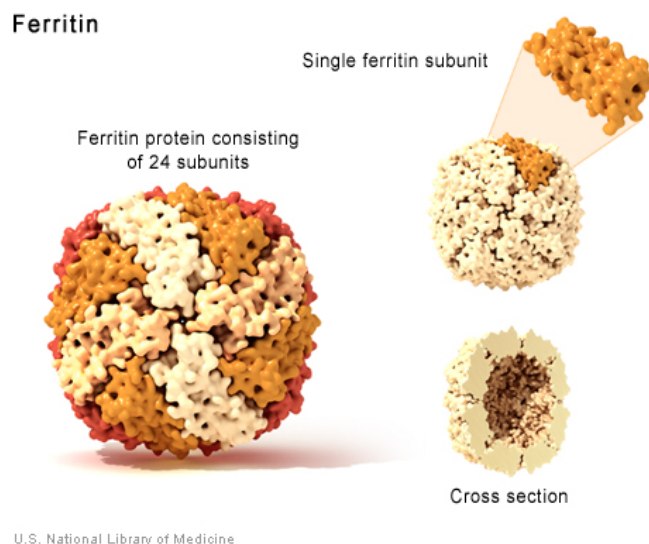


Figure 1.2 An illustration of the protein shell of a ferritin molecule. The outer diameter is 10-12 nm with an inner diameter of 6-8 nm. The shell contains 24 protein subunits with 26 channels at the intersections of these subunits. (Graphic obtained from <http://www.geneticsolutions.com>)

the shells, 3) the commercial availability of processed ferritin, and 4) the readily functionalized nature of the protein shells, ferritin molecules could serve as excellent biological-delivery vehicles for near-ideal nanotube catalysts.

1.5 Previous Research in Ferritin Catalysts

The first group to investigate ferritin as a nanotube catalyst was Dai *et al.* at Stanford University in 2001 [8]. They started with apoferritin and produced a sample that contained 200 Fe atoms inside the core and another sample that contained 1100 Fe atoms in the core. After using these samples to grow carbon nanotubes on silicon wafers and ultrathin Al_2O_3 transmission electron microscope membranes, they imaged the nanotubes and particles using both an Atomic Force Microscope (AFM) and a Transmission Electron Microscope (TEM). They obtained a relatively narrow diameter distribution in the nanotubes and very clear TEM images of SWNT grown

directly from discrete ferritin cores. While these findings are very impressive and potentially beneficial, there appears to be some difficulty in replicating their results.

In their report, Dai *et al.* claim that after deposition the individual ferritin molecules remain isolated and do not clump together. Their initial TEM analysis of the ferritin deposition was done on carbon membranes that break down and evaporate at high temperatures (above 500°C). For this reason, they used ultrathin Al₂O₃ membranes for their nanotube growth and subsequent TEM imaging of the nanotubes. These membranes are very porous and may have contributed to the isolation of the iron nanoparticles. To understand the distribution of the ferritin cores for growths done on silicon wafers, the size of the nanoparticles after calcination (heating to 800°C for 5 min to remove the organic shell of the ferritin) were measured using an AFM. In these measurements it was assumed that the nanoparticles were spherical so that their lateral width could be obtained from their vertical height. If each particle truly came from only one ferritin core then this may be an accurate assumption, but if the ferritin cores were occasionally clumped then this assumption could be inaccurate.

In 2002, Bonard *et al.* in Lausanne Switzerland used ferritin to catalyze the growth of thin and monodisperse multiwalled nanotubes [12]. Upon attempting to deposit the ferritin and grow nanotubes, they discovered that the resultant nanotubes had an extremely broad distribution in diameters. After analyzing these samples in the TEM, they determined that the nanoparticles had diffused and coalesced together to form large particles that then served as the catalyst for the nanotubes. To avoid this agglomeration (clustering into a mass of particles) and amalgamation (consolidation into a unified or integrated whole) they attempted to hinder the mobility of the particles by imbedding them in a Al(NO₃)₃·9H₂O matrix that was stable and inert at the growth conditions. This process succeeded in drastically decreasing the agglomeration of the particles, and they were able to obtain fairly discrete cores with a mean

diameter of 4.9 nm and a spread of 1.1 nm. However, the presence of the supporting matrix limited the number of catalyst particles that were exposed to the hydrocarbon gas. Consequently, only about 25 percent of the iron cores produced nanotubes.

Another group, at Kumamoto University in Japan, attempted to use ferritin to obtain lattice-oriented growth of nanotubes on a gold surface [13]. This group used ferritin that contained larger iron cores than previous groups (6 ± 2 nm) and a fairly dense deposition density. They removed the carbon shells of the ferritin before the nanotube growth process by heating the samples to 400°C for 60 min. The nanotubes that resulted from this process had average diameters (6 ± 2 nm) that were very similar to the diameters of the catalyst particles; however, this size distribution is very large.

A second group in Japan, Jeong *et al.*, directly studied the relationship between the density of the catalyst particles and the resulting diameters of the nanotubes [14]. They also removed the protein shell of the ferritin by calcinations (450°C, 5 min) prior to the CVD growth process. After growing SWNT they recognized that the aggregation of the iron cores at high growth temperatures (900°C) contributed to the wide diameter distributions they obtained. This observation was supported by experiments showing that when the density of the catalyst nanoparticles was decreased, the SWNT were more homogeneous. From their results they arrived at the following conclusion: “*From the systematic growth and analyses using different nanoparticles densities and substrates, we can understand that the agglomeration of discrete nanoparticles should be suppressed for nanotube growth with narrow diameter distribution*” [14](Italics added).

1.6 Research Goals

The research that is summarized above shows that ferritin can be used as an effective catalyst for CVD SWNT growth. However, many of these researchers recognized that the catalyst's density and freedom of movement contribute to a disappointingly wide distribution in the resulting nanotube diameters. Most groups studied the individual particle size and overall distribution of the ferritin prior to their exposure to high temperatures. Yet, despite recognizing the importance of consistency in catalyst size and even the potential for catalyst amalgamation, these groups focused on the distributions of the resulting nanotubes and failed to adequately determine catalyst particles' characteristics after their exposure to nanotube growth temperatures.

In my research, I expose the ferritin catalyst to nanotube growth temperatures and seek to learn what is happening to the particles as they are deposited and annealed. To accomplish this purpose, I focus on how the ferritin molecules react with the substrate and each other, both as they are deposited and as they are heated to temperatures between 600°C and 800°C. I find that 1) restricting the deposition time and rinsing the sample increases consistency in the density and decreases the amalgamation of the iron cores, 2) the nature of the substrate has a significant effect on the density of the deposited ferritin, 3) the presence of the protein shells in the heating process increases the mobility of the iron cores, 4) an oxygen plasma cleaner can remove the protein shells without impacting the positioning of the iron cores, 5) ferritin cores that are clustered together before heating can remain separate from one another above 700°C, if their cores have been removed by an oxygen plasma cleaner. However, it is unlikely that they will remain discrete at temperatures in excess of 800°C.

Chapter 2

MATERIALS AND METHODS

2.1 Imaging Equipment

Previous investigations in the use of ferritin as a nanotube catalyst have relied heavily on Atomic-Force Microscopy (AFM) and High-Resolution Transmission Electron Microscopy (HRTEM) to image the ferritin. However, both of these methods have intrinsic faults that limit their usefulness in studying ferritin. Atomic-force microscopy produces images by passing a silicon tip over a surface and using a laser to measure the vertical displacement of the tip as it encounters objects on that surface. This process produces extremely accurate information on the vertical topography of the sample, but the lateral resolution is seriously impaired by the width of the tip, which can be 15-20 nanometers wide. The limitations on the AFM's lateral resolution is not very important in the imaging of cylindrical nanotubes that are lying flat on a surface. However, when the lateral dimensions of a sample cannot be assumed by symmetry, this characteristic of AFM's can make size measurements very difficult and inaccurate. Since it is generally assumed that it is the lateral dimensions, not the vertical height, of the iron cores that directly affects the diameters of the nanotubes

that are grown from them, AFM's lateral imaging weaknesses seriously limit their usefulness for catalyst imaging.

Transmission Electron Microscopy (TEM), in which an accelerated beam of electrons passes through a very thin sample, has excellent lateral resolution capabilities. However, the image obtained by the TEM is dependant on the diffraction of the electron beam from the crystalline objects in the sample. Therefore, it is very difficult to distinguish the iron cores, which are approximately 5 nanometers in size, from the 40 to 100 nanometer thick substrate that supports them. In addition, the thin, amorphous, protein shells contribute almost nothing to the diffraction of the beam. Consequently, these shells are essentially invisible in almost any form of transmission electron microscopy.

HRTEM is a high magnification mode available on many transmission electron microscopes. The high magnifications provided by HRTEM enable the viewing of the diffraction lines from individual ferritin cores. But the very nature of high magnification severely limits the microscopes field of view to only a few ferritin cores at a time. Therefore, HRTEM cannot produce a large-scale image of the ferritin density.

These three forms of microscopy (AFM, TEM, and HRTEM) have many useful applications. However, to understand the deposition and movement of the ferritin cores, we needed an imaging method that could provide accurate information on both the lateral sizes of the particles and their global distribution.

To accomplish our imaging needs, we relied heavily on the use of Scanning Transmission Electron Microscopy (STEM). STEM differs from regular TEM in that the electron beam is focused to a sub-nanometer spot on the surface of the sample and then quickly scanned across the surface. At each point on the surface a High Angle Annular Dark Field (HAADF) Detector records the number of electrons that are scattered to relatively large angles. A computer then translates this data to an intensity

that is displayed on a computer monitor. Since atoms with a larger atomic number have a greater impact on the trajectory of the electron beam, the intensity recorded by the detector is proportional to $Z^{1.7}$, where Z is the atomic number of the target atoms at the beam location. The contrast in the resulting image is related to the ratio $\frac{N_1 Z_1^{1.7}}{N_2 Z_2^{1.7}}$, where N_1 and N_2 represent the atomic densities of two materials and Z_1 and Z_2 represent their respective atomic numbers. The large difference between the atomic number of iron cores ($Z_{Fe} = 26$) and that of the silicon nitride membrane ($Z_{Si} = 14$ and $Z_N = 7$) allows us to clearly distinguish the iron cores of the ferritin from the background material.

All of the STEM imaging was done on the Tecnai F-20 (Fig. 2.1) microscope in the underground lab of the Eyring Science Center at BYU. Some of the ferritin samples were placed on copper grids coated with a carbon membrane (Ted Pella Inc., 01800-F). Since the carbon membranes decompose and evaporate at temperatures above 450°C , all of the annealed samples were placed on Silicon Nitride (Si_3N_4) membranes. Both 50 nm (SPI Supplies, 4124SN) and 100 nm (SPI Supplies, 4122SN) thick silicon nitride membranes were used in our experiments. However, due to the uneven background produced by the 50 nm films, the majority of the experiments were performed using the 100 nm silicon nitride membranes.

2.2 Early Experiments

To gain an initial understanding of how ferritin molecules interact with one another at the temperatures typically used for nanotube growth, a simple test was first attempted, with rather surprising results. A drop of 1.82 mg/mL ferritin was placed on a 100 nm thick silicon nitride membrane and then the excess liquid was drawn off with filter paper. Fig. 2.2 shows a STEM image of the deposition density. The small



Figure 2.1 Tecnai F-20 Analytical STEM microscope. Located in the Eyring Science Center’s underground lab on Brigham Young University’s campus in Provo, Utah.

bright dots are the iron cores of the ferritin while the larger bright objects are mostly dense clumps of ferritin. After imaging, the sample was annealed at 800°C for 15 minutes.

We were surprised to find that the iron cores of the ferritin molecules had amalgamated together to form large crystals that were several microns in size (Fig. 2.3). Since 800°C is only roughly half the melting temperature of iron, the iron atoms should have a diffusion length that is very short and the growth of crystals this size should not result. For amalgamation of the iron to occur on this scale, the iron particles would need to have first formed large clumps by some means other than the atomic diffusion of iron atoms.

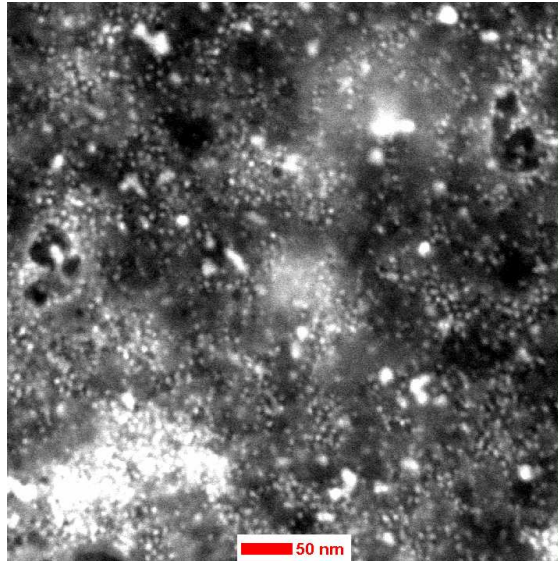


Figure 2.2 High density ferritin deposition on Si_3N_4 . Deposited using a preliminary deposition technique. The bright spots are individual ferritin and clumps of ferritin in varying quantities (90 kx magnification)

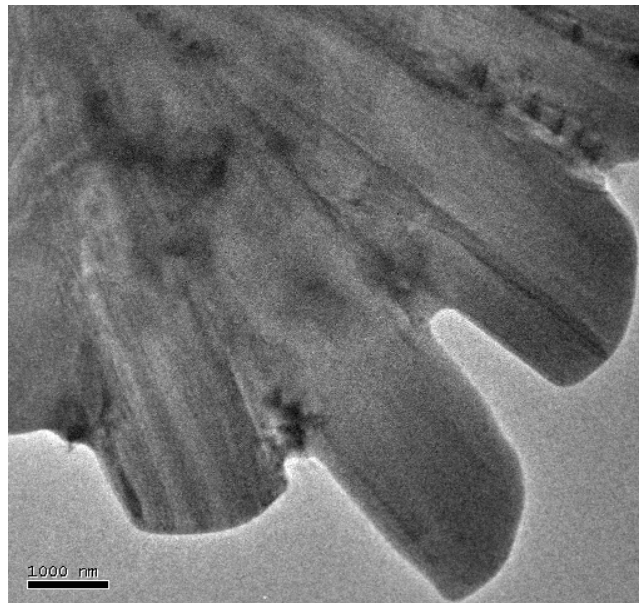


Figure 2.3 TEM image of a large iron crystal obtained after annealing the high density ferritin at 800 °C for 10 minutes. (59 kx magnification)

2.3 Obstacles: Density, Movement, and Heat

We concluded that there were two major causes of the catalyst amalgamation. First, the ferritin was clearly too densely deposited on the substrate. Second, the movement of the melting protein shells led them to clump together, causing a drastic aggregation of the iron cores. To solve these problems we focused on decreasing the density of the deposited ferritin and finding a method to remove the protein shells from the ferritin cores without allowing them to move. We then annealed the ferritin samples at a variety of temperatures to determine the temperature at which the transition from discrete iron cores to amalgamated particles occurs.

2.4 Ferritin Deposition Process

For our experiments we used horse-spleen ferritin with a concentration of 91 mg/mL in a 0.15M sodium chloride solution (Sigma Chemical, St Louis MO). Most of the ferritin that we used was mixed in two batches. The first batch was mixed by a BYU graduate student, Degao Xu, on 8 March 2004 using a 0.05M phosphate buffer (pH 7.4) that contained 0.05M NaCl to achieve several desired concentrations (0.01 mg/mL, 0.1 mg/mL, 1 mg/mL, and 10 mg/mL) [15]. The second batch was mixed by Mark Esty on 9 November 2005, using high-purity water to achieve a concentration of 1 mg/mL. Both batches were refrigerated at 4°C when not in use. The deposition densities of the two batches of ferritin appear to be very similar when they are deposited using identical processes.

To decrease the density of the deposited ferritin, we modified a deposition process that was suggested by Degao Xu [15]. We will hereafter refer to this process as our “standard deposition technique.” It is outlined as follows:

- 1) Place a drop of ferritin on a substrate using a pipette with a disposable tip.

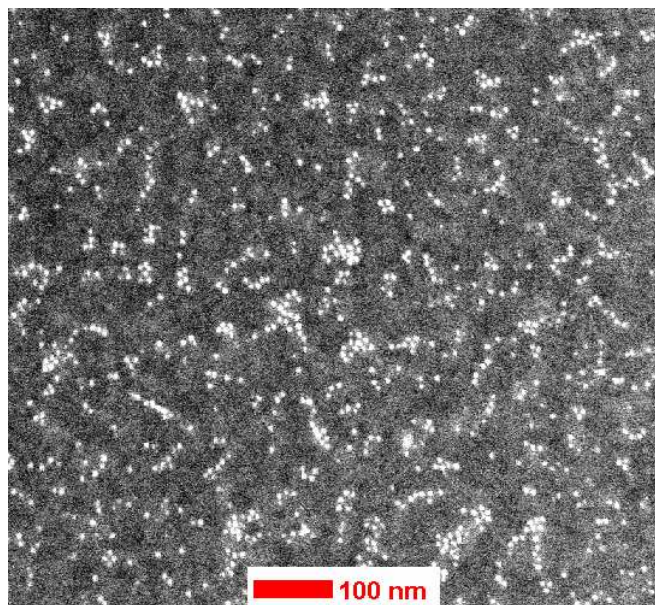


Figure 2.4 The ferritin concentration on silicon nitride using the standard deposition technique. Each bright dot is an individual iron core inside a ferritin molecule. (205 kx magnification)

- 2) Allow the ferritin to remain on the surface for a specified period of time, typically 30 seconds.
- 3) Dip the sample in high-purity water and rinse for 30 seconds.
- 4) Gently blow nitrogen gas on the sample to dry it.

We have discovered that using ferritin with a 1 mg/mL concentration and leaving the ferritin on the substrate for 30 seconds before rinsing produces a fairly evenly dispersed sub-monolayer of ferritin on a silicon nitride surface (Fig. 2.4).

2.5 Importance of Substrate on Density

By using several different TEM membranes we discovered that the nature of the substrate has a significant impact on the density of the deposited ferritin. Fig. 2.5 shows the density of ferritin that was deposited on a carbon film using a process

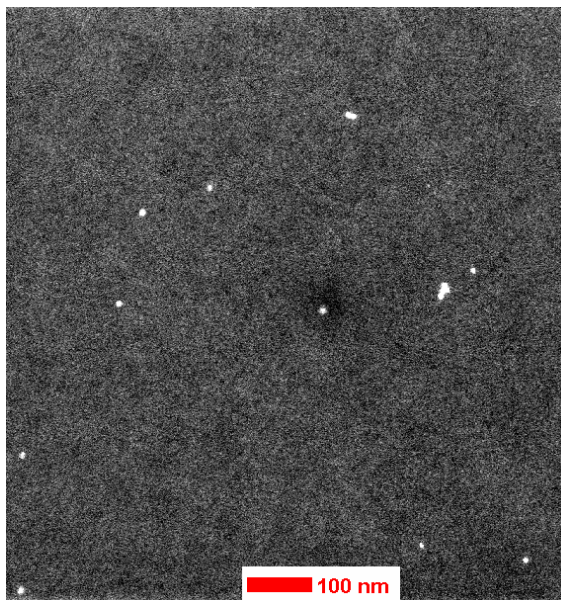


Figure 2.5 Ferritin concentration on a carbon membrane using the standard deposition technique. Notice the significant decrease in ferritin concentration compared to an identical deposition on silicon nitride (Fig. 2.4). (205 kx magnification)

identical to the one used to deposit ferritin on the silicon-nitride film in Fig. 2.4. This same dependence on the substrate was noticed by Li *et al.* [8]. They pre-wet the carbon grid with methanol to overcome the highly hydrophobic nature of the carbon film. The contrast between the ferritin density on carbon with that on silicon nitride is important because carbon grids are the most common TEM membranes, but nanotube growths have historically been performed on silicon wafers. To ensure that there is continuity between the ferritin density on silicon nitride that we are studying and the density that will be used in the growth processes, we manufactured several silicon dioxide TEM membranes. By comparing the ferritin density on these membranes with the density on silicon nitride membranes from SPI, we determined that there was very little variance between silicon dioxide and silicon nitrite and that continuity could be assumed (Fig. 2.6).

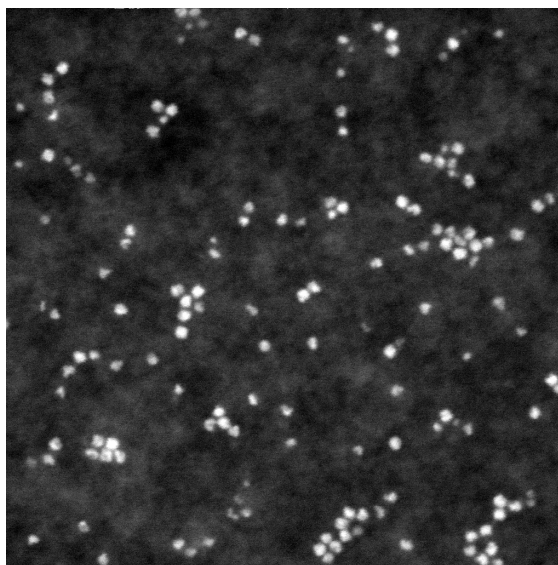


Figure 2.6 Ferritin concentration on a silicon dioxide membrane using the standard deposition technique. While the magnification is higher than Fig. 2.4, notice the similarities in the density of the iron cores. (580 kx magnification, individual iron cores are approximately 4-6 nm)

2.6 Plasma Cleaning

In most of the previous experiments [8, 14], the protein shells were removed from the iron cores by heating the samples to temperatures above 450°C for an extended time. Because we believed that temperatures near the melting point of the shells were contributing to the aggregation of the ferritin, we decided to remove the shells before heating and test the validity of our predictions. To remove the protein shells from the iron cores without heating the samples, we used a plasma cleaner (Fig. 2.7) which removes carbon contamination from TEM samples by exposing them to an oxygen plasma. Most of the samples that were plasma cleaned were exposed to the plasma for five minutes. However, exposure times of about one minute appear to be sufficient for removing the majority of the carbon.

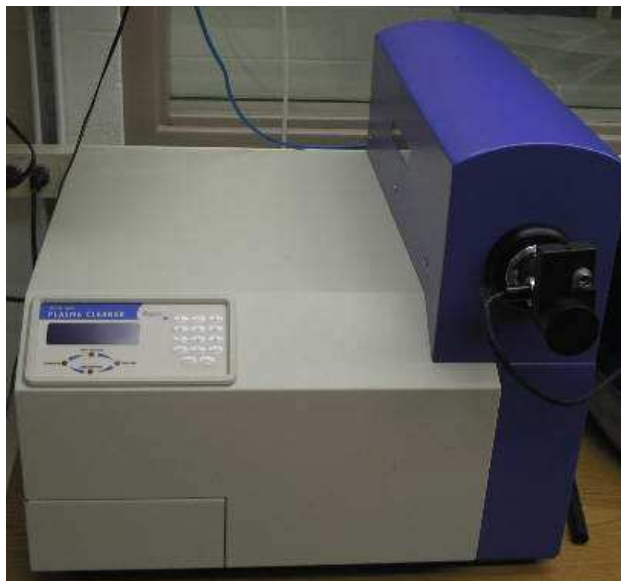


Figure 2.7 Fischione Instruments model 1020 Plasma Cleaner that is used to clean carbon from TEM samples. A TEM sample holder is shown inserted into the instrument on the right, front face.

2.7 Annealing Process

To anneal the ferritin samples we use a tube furnace (Lindberg/Blue M, TF55030COM A-1) with a quartz tube (1" X 24") and a quartz slide. The silicon dioxide membranes are placed on the quartz slide under a flow of 500 standard cubic centimeters per minute (sccm) of argon gas. After the furnace is heated to the desired temperature (600°C or 800°C) the samples are held at that temperature for 10 minutes. The furnace is then turned off and allowed to cool to under 90°C before the gas is turned off and the samples are removed.

Chapter 3

RESULTS AND CONCLUSIONS

3.1 Effect of Ferritin Proximity on Amalgamation

In our early experiments, we found that a dense distribution of ferritin on a surface can drastically increase the clumping of the iron cores. To help resolve this problem and keep the ferritin cores discrete at high temperatures, we dramatically decreased the density of the deposited ferritin.

However, even after we decreased the density, many of the ferritin molecules formed small clusters or chains (Fig. 3.1). In addition, large agglomerations of ferritin would occasionally form during the deposition process (Fig. 3.2). As seen in Fig. 3.3, even when these clumps are annealed at a relatively low temperature (600°C), the close proximity of the iron cores encouraged them to diffuse together and form relatively large crystals of iron.

The smaller clusters and chains did not create extremely large crystals of iron; however, the iron cores in these molecules did combine with their nearest neighbors to form particles that consisted of two to six ferritin cores. The clumping of the iron cores can be seen by comparing Fig. 3.4 to Fig. 3.5. In the annealed sample the

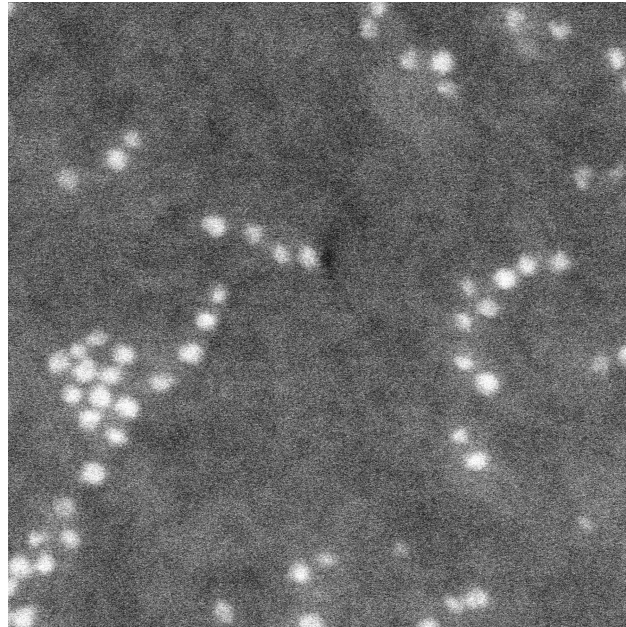


Figure 3.1 Ferritin on a silicon nitride film. The ferritin molecules tend to automatically form small clusters and chains. This sample has not been annealed. (810 kx magnification)

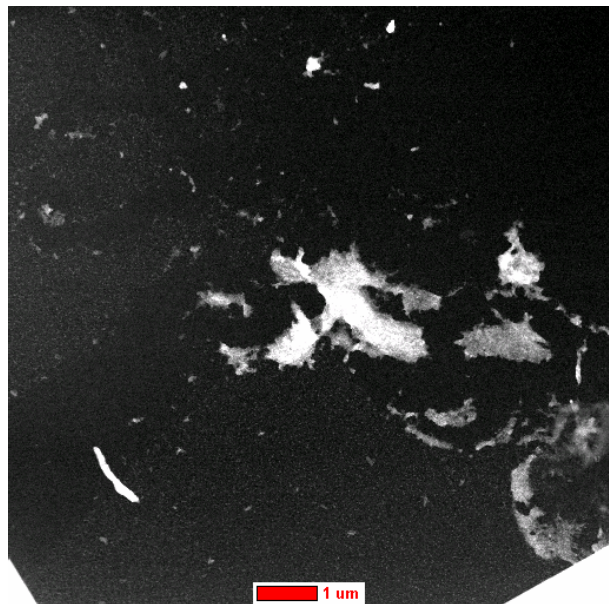


Figure 3.2 A dense clump of ferritin molecules on a silicon nitride surface. This sample has not been annealed. (81 kx magnification)

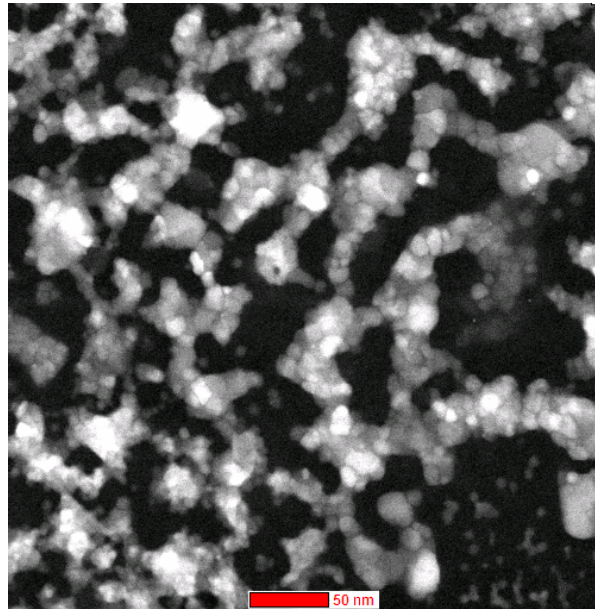


Figure 3.3 Iron crystals formed at 600°C from a dense clump of ferritin. This sample was plasma cleaned and annealed at 600°C. (410 kx magnification)

spacings between the particles (as well as the particles themselves) are larger and more random in size.

When there is contact between the shells of several ferritin molecules before the annealing process, the cores will have a high probability of diffusing into larger particles. There is also a relationship between the number of ferritin molecules in a cluster and the probability of that cluster becoming a conglomerate of particles. For example, Fig. 3.6 shows a pair of ferritin cores that have remained discrete after being annealed at 800 °C when larger clusters that were prepared under more optimum circumstances (Fig. 3.3) formed larger particles.

3.2 Effect of Plasma Cleaning

While the proximity of the neighboring ferritin molecules has a large impact on the probability of a particular iron core becoming part of a larger particle, the actual

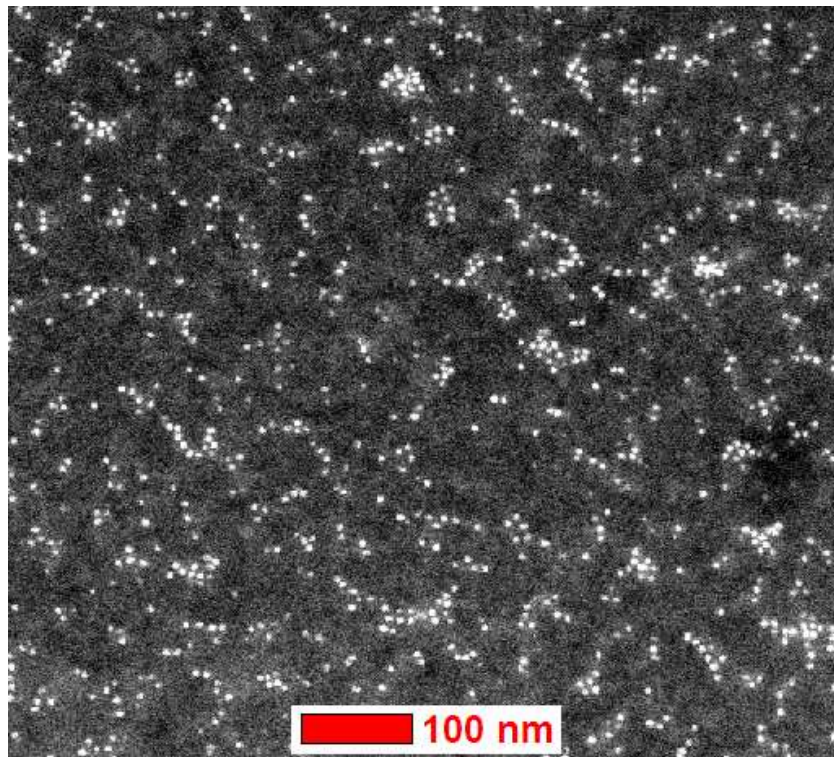


Figure 3.4 Ferritin molecules deposited on a silicon nitride film. This sample has not been plasma cleaned or annealed. Notice the regular spacing between the discrete iron cores within clumps and chains. (205 kx magnification)

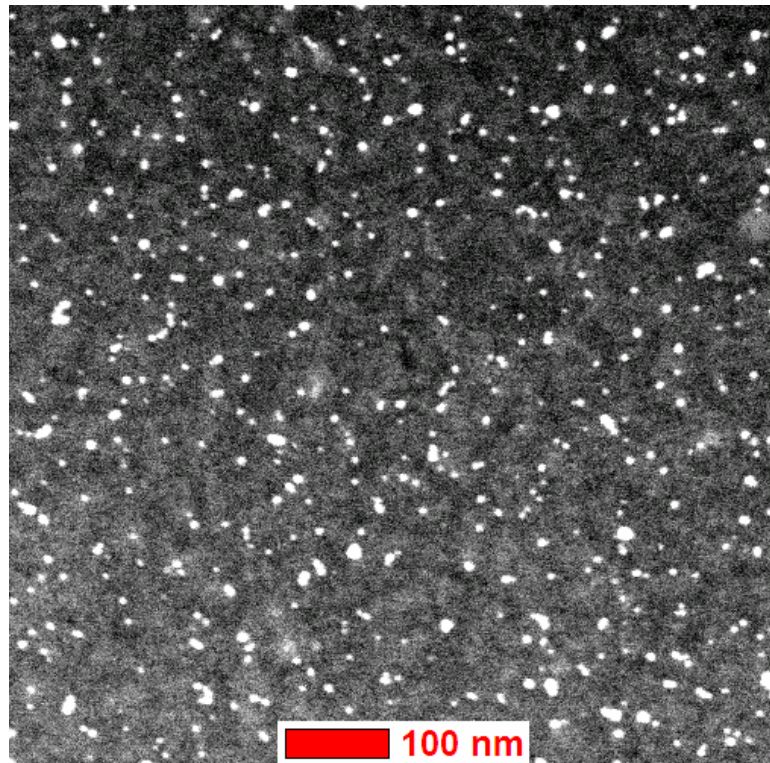


Figure 3.5 Ferritin molecules deposited on silicon nitride and annealed at 600°C without any plasma cleaning. Many of the clusters and chains in Fig. 3.4 have merged together to form larger particles. Notice the increased spread in particle size and the decrease in regular spacing within clumps and chains. (205 kx magnification)

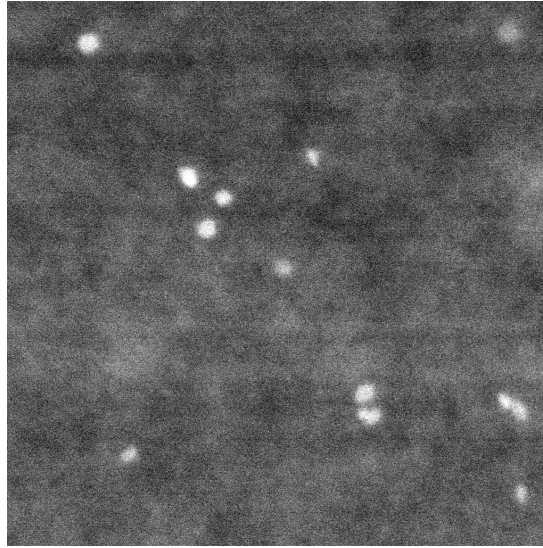


Figure 3.6 Ferritin cores deposited on silicon nitride and annealed at 800°C without any plasma cleaning. The bright iron cores are approximately 5 nm in size and may have remained discrete due to the relatively small size of the clumps (two or three iron cores). (810 kx magnification)

movement is the result of two processes: 1) the melting of the protein shells, creating liquid droplets that bring together the core particles before the carbon evaporates, and 2) the atomic diffusion of iron atoms across the distance that separates the particles from their nearest neighbors. This atomic diffusion length can be affected by a variety of factors including the particle's composition, the nature of the substrate, the temperature, and the environmental conditions surrounding the particle.

To test the hypothesis that the ferritin shells increase the mobility of the iron cores, we removed the protein shells before the annealing process using a TEM plasma cleaner. By imaging the samples before (Fig. 3.7) and after (Fig. 3.8) exposing them to five minutes of plasma cleaning we determined that the positions of the iron cores were not affected by the plasma processing.

Fig. 3.9 shows a sample that has been plasma cleaned and then annealed at 600°C. When this sample is compared to a sample that has been annealed at 600°C without

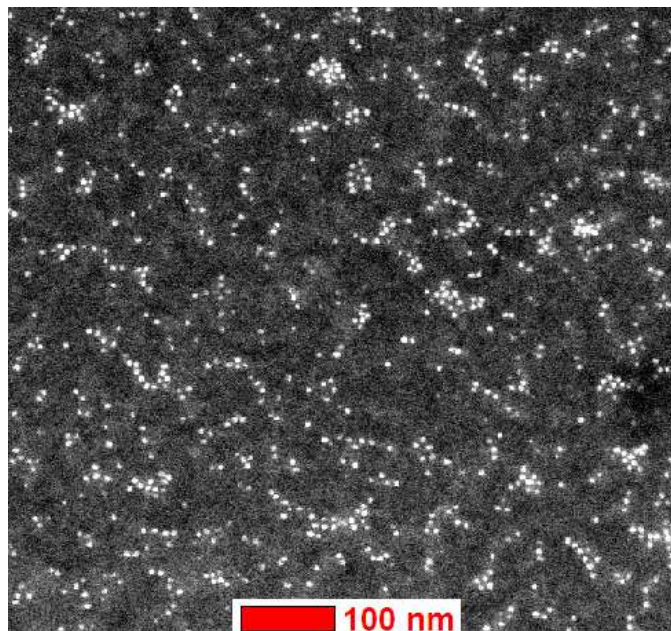


Figure 3.7 Ferritin deposited on a silicon nitride surface. This sample has not been plasma cleaned or annealed. (205 kx magnification)

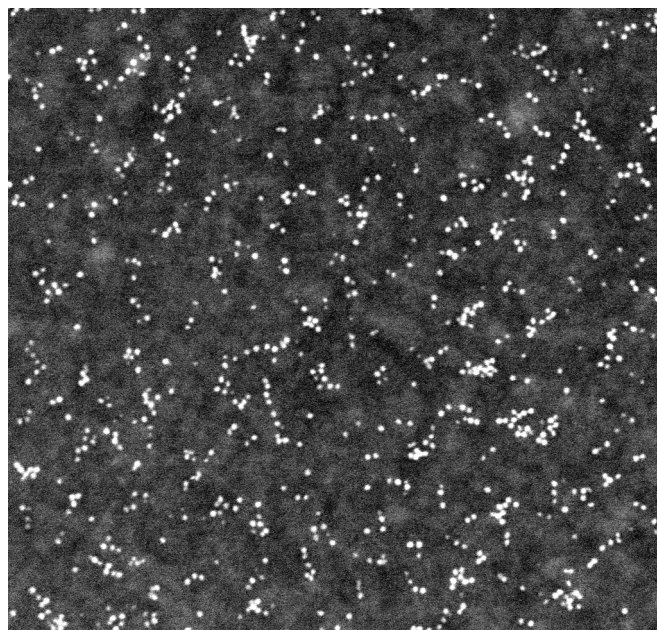


Figure 3.8 Iron nanoparticles derived from ferritin after their protein shells have been removed by a 5 minute exposure to an oxygen plasma. When compared to Fig. 3.7 it is clear that the relative positions of the iron cores have not been affected by the plasma. (205 kx magnification)

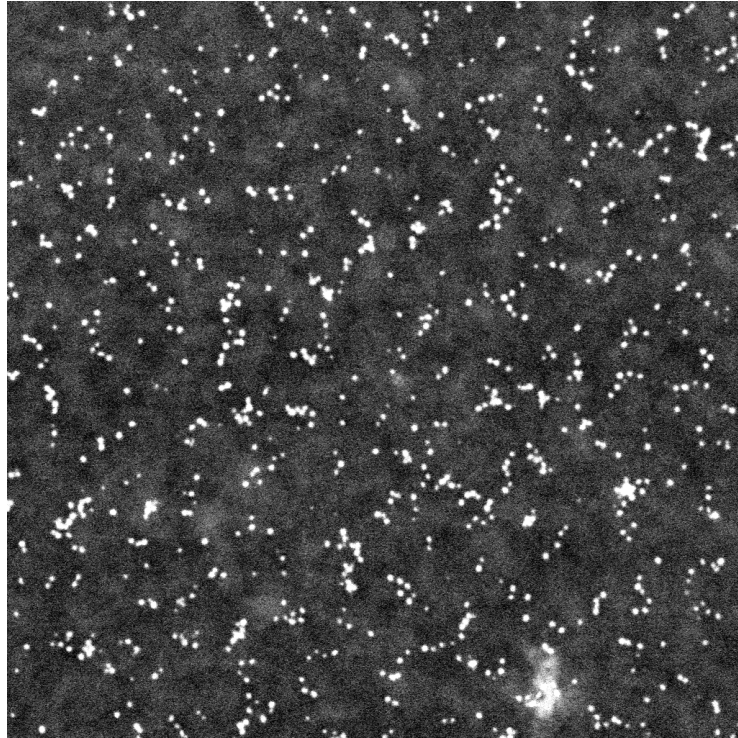


Figure 3.9 Ferritin nanoparticles that have been plasma cleaned and then annealed at 600°C. The majority of the particles have retained their relative positions within the chains and small clusters without diffusing into larger particles, especially when compared to Fig. 3.10. (205 kx magnification)

being plasma cleaned (Fig. 3.10), it can be seen that the plasma-cleaned sample has greater consistency in particle size and spacing.

While the plasma cleaning process decreases the mobility of the iron cores and increases particle consistency, it does not completely eliminate the amalgamation of the iron cores. The sample in Fig. 3.3 was plasma cleaned before being annealed, but where the ferritin was deposited in large clumps the iron cores still amalgamated to form larger particles. To understand the limitations of plasma cleaning, we compared samples that had been annealed at 800°C both with and without being plasma cleaned. The sample in Fig. 3.11 was plasma cleaned before it was annealed at 800°C. From the image it is clear that the spread in particle size has increased and

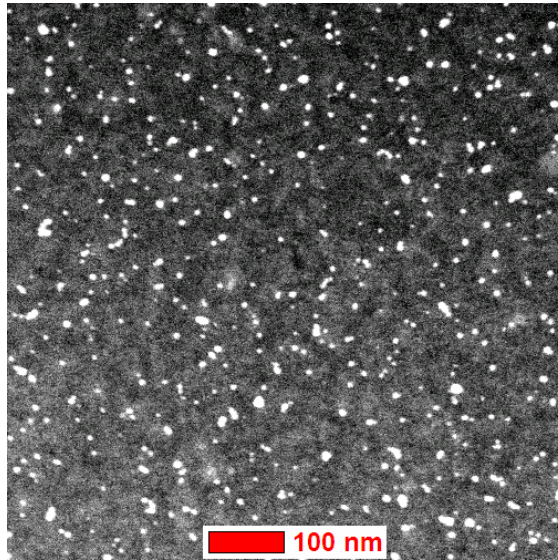


Figure 3.10 Ferritin-core nanoparticles that have been annealed at 600°C without being plasma cleaned. Many of the clusters and chains in Fig. 3.9 have merged together to form larger particles. Notice the increased spread in particle size and the decrease in regular spacing within clumps and chains. (205 kx magnification)

the spacing between the particles has become larger and more random. The prior existence and distribution of the ferritin clumps and chains can be implied from the image; however, these chains and clumps have been significantly altered during the annealing process. The impact of the plasma cleaner in decreasing particle movement becomes overshadowed by short-range atomic diffusion as the annealing temperature increases.

3.3 Diffusion Length

When the protein shell of a ferritin molecule is removed during plasma cleaning the core settles to the surface of the substrate with little or no horizontal displacement. Therefore, the average distance between iron nanoparticles is the combined thickness of the two shell walls that separated them (approximately 4 nm). In contrast, when

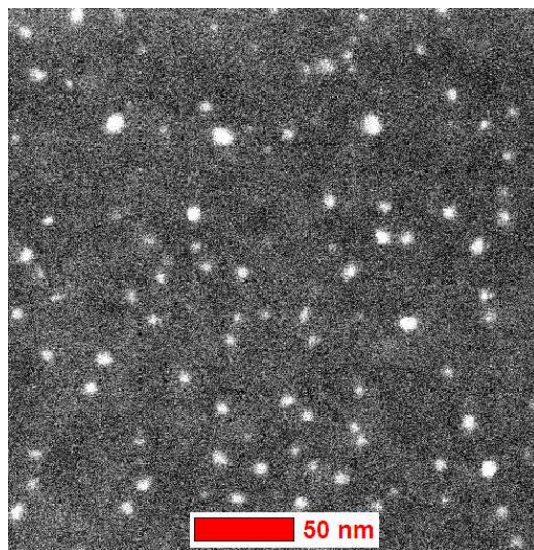


Figure 3.11 Ferritin-core nanoparticles that have been plasma cleaned and then annealed at 800°C. Notice the increased spread in size and spacing when compared to the sample annealed at 600°C (Fig. 3.10). (410 kx magnification)

the shells are removed using calcination (heating at 500°C), there is an increased probability of horizontal core movement that is likely to reduce the distance between nearest-neighbor particles to under 4 nm.

Once the protein shells have been removed, particle amalgamation is dominated by the atomic diffusion of the individual iron atoms. Near 600°C the diffusion length of these atoms appears to be smaller than the 4 nm average distance between particles, and therefore the majority of the nanoparticles remain discrete from one another. However, near 800°C this atomic diffusion length has increased and appears to exceed the average distance between the iron cores.

Within the larger clumps of ferritin, some of the cores appeared to be separated by less than 4 nm both before and after being plasma cleaned. This could indicate that not all of the molecules were located in the same lateral plane and that some of the molecules may have been resting above others before the shells were removed. In this situation the final lateral distance between cores after plasma cleaning would be

less than 4 nm. This could explain some of the amalgamation that occurred in the plasma cleaned sample that was annealed at 600°C.

3.4 Conclusions

We have found that the protein shells of the ferritin molecules increase the agglomeration of the iron-core nanoparticles when the samples are annealed to temperatures in excess of 600°C. By removing these shells using an oxygen plasma cleaner, particle movement has been reduced to where the diffusion length of the iron atoms between the neighboring cores is the primary mechanism of particle growth. At 600°C this atomic diffusion length appears to be slightly less than twice the thickness of the ferritin molecules' protein shells (4 nm) and at 800°C the diffusion length appears to exceed 4nm. However, even near 600°C, a below-average distance between two particles in a larger clump may cause one particle to increase in size and eventually absorb its nearest neighbors through diffusion.

Plasma cleaning holo-ferritin molecules can decrease their agglomeration during the heating process without significantly altering the dispersion of the iron core nanoparticles. If these particles are more than 4 nm apart after the plasma cleaning they are likely to remain discrete from one another near 600°C, but any benefit derived from the plasma cleaning appears to be lost near 800°C. To use ferritin molecules to create well-defined catalyst particles nanotube growths should be performed near 600°C and the distance between ferritin cores should be greater than 4 nm.

Bibliography

- [1] M.-F. Yu, O. Lourie, M. J. Dyer, K. Moloni, T. F. Kelly, and R. S. Ruoff, “Strength and Breaking Mechanism of Multiwalled Carbon Nanotubes Under Tensile Load,” *Science* **287** (2000).
- [2] W. Wu, S. Wieckowski, G. Pastorin, M. Benincasa, C. Klumpp, J.-P. Briand, R. Gennaro, M. Prato, and A. Bianco, “Targeted Delivery of Amphotericin B to Cells by Using Functionalized Carbon Nanotubes,” *Angew. Chem. Int. Ed.* **44** (2005).
- [3] P. L. McEuen, “Single-wall carbon nanotube,” *PHYSICS WORLD* **13**, 31–36 (2000).
- [4] R. F. Curl, “Dawn of the Fullerenes: Conjecture and Experiment (Nobel Lecture),” *Angew. Chem. Int. Ed. Engl* **36** (2003).
- [5] P. L. McEuen, M. S. Fuhrer, and H. K. Park, “Single-walled carbon nanotube electronics,” *IEEE TRANSACTIONS ON NANOTECHNOLOGY* **1**, 78–85 (2002).
- [6] H. Dai, “Controlling nanotube growth,” *PHYSICS WORLD* **13**, 43–47 (2000).

-
- [7] L. An, J. M. Owens, L. E. McNeil, and J. Liu, "Synthesis of Nearly Uniform Single-Walled Carbon Nanotubes Using Identical Metal-Containing Molecular Nanoclusters as Catalysts," *J. Am. Chem. Soc.* **124**, 13688–13689 (2002).
- [8] Y. Li, W. Kim, Y. Zhang, M. Rolandi, D. Wang, and H. Dai, "Growth of Single-Walled Carbon Nanotubes from Discrete Catalytic Nanoparticles of Various Sizes," *J. Phys. Chem. B* **105**, 11424–11431 (2001).
- [9] M. Ishida, H. Hongo, F. Nihey, and Y. Ochiai, "Diameter-Controlled Carbon Nanotubes Grown from Lithographically Defined Nanoparticles," *Jpn. J. Appl. Phys.* **43**, 1356–1358 (2004).
- [10] J. L. Johnson, "Non-Redox Iron Release Kinetics of Horse Spleen Ferritin," Honors Thesis, Department of Chemistry and Biochemistry, Brigham Young University (1995).
- [11] D. D. Brosnahan, "Phosphate and Ferritin Iron Deposition," Honors Thesis, Department of Chemistry and Biochemistry, Brigham Young University (2000).
- [12] J.-M. Bonard, P. Chauvin, and C. Klinke, "Monodisperse Multiwall Carbon Nanotubes Obtained with Ferritin as Catalyst," *Nano Letters* **2**, 665–667 (2002).
- [13] M. Tominaga, A. Ohira, A. Kubo, I. Taniguchi, and M. Kunitake, "Growth of carbon nanotubes on a gold (111) surface using two-dimensional iron oxide nanoparticle catalysts derived from iron storage storage protein," *Chem. Commun.* pp. 1518–1519 (2004).
- [14] G.-H. Jeong, S. Suzuki, Y. Kobayashi, A. Yamazaki, and K. Homma, "Effect of nanoparticle density on narrow diameter distribution of carbon nanotubes and particle evolution during chemical vapor deposition growth," *J. App. Physics* **98**, 124311 (2005).

- [15] D. Xu, "Atomic Force Conductivity Measurements of Single Ferritin Molecules," Masters Thesis, Department of Physics and Astronomy, Brigham Young University (2004).

Index

Agglomeration, 7
Amalgamation, 7
Annealing, 19
Apoferitin, 5
Atomic-Force Microscopy (AFM), 10

Chemical Vapor Deposition (CVD), 3

Ferritin, 5
Ferritin deposition, 15
Ferritin, Image, 6

High-Resolution Transmission Electron Microscopy (HRTM), 11
Holoferitin, 5

Nanotubes, Background, 2
Nanotubes, Image, 2

Plasma Cleaner, 18

Scanning Transmission Electron Microscopy (STEM), 11
Single-Walled Nanotubes (SWNT), 2
Standard deposition, 15

Transmission Electron Microscopy (TEM), 11